Conformational Preference in Heteroatomic Analogues of Ethane, H_3X-YH_3 (X = B, Al; Y = N, P): Implications of Charge Transfer

Sairam S. Mallajosyula, Ayan Datta, and Swapan K. Pati*

Theoretical Sciences Unit and DST Unit on Nanoscience, Jawaharlal Nehru Center for Advanced Scientific Research, Jakkur Campus, Bangalore 560 064, India

Received: December 30, 2005; In Final Form: February 21, 2006

Quantum chemical conformational analysis for electron donor−acceptor (EDA) systems, H_3B-NH_3, H_3B-PH_3, H_3Al-NH_3 and H_3Al-PH_3, has been performed. For H_3B-NH_3 and H_3B-PH_3, the rotational barrier is found to be invariant with an increase in the central bond (X−Y) length. For H_3Al-NH_3 and H_3Al-PH_3, however, the rotational barrier increases with an increase in the central bond length. Decomposition of the total energy into various components and their contributions to the frontier orbitals (HOMO, HOMO−1, HOMO−2 and HOMO−3) have been analyzed in detail to explain the origin of such anomalous changes in the rotational barrier. Charge transfer and favorable "back bonding" are found to be the crucial factors governing the variations in the rotational barrier for such systems.

1. Introduction

Molecular conformation is of fundamental importance in quantifying the structure−property relationship of chemical processes. Conformational preference is intimately connected with the properties of simple molecules[1] as well as that for macromolecules, polymers and proteins.[2] Conformational preferences arise due to special stabilities at certain angular orientations compared to other angles. Steric repulsions between the neighboring atoms in the eclipsed conformer that are relieved in the staggered conformer have been generally understood to be the origin of such staggered preference.[1,3] However, recently, there has been a renewed interest in the search for the origin of such conformational preference in organic homo-binuclear molecular systems[4−9] as conformational flexibility amounts to one of the basic processes in structural chemistry.

Heteronuclear molecules with electron donor−acceptor (EDA) characteristics also show a similar conformational preference[10−12] with the staggered form being the most stable conformation. Conformational preference for EDA molecule like H_3B-NH_3 has been recently reported.[13] Similar studies on the structural aspects of many other EDA complexes are also well-reported,[13−16] with donor as NH_3 or PH_3 and acceptor as BH_3 or AlH_3. However, a systematic and complete study for the relationship between the rotational barrier and the extent of charge transfer between the donor and the acceptor fragments is clearly missing in the literature. For a clearer understanding of the molecular electronic mechanisms governing the conformational preferences in these EDA systems, we have chosen a series of systems (H_3B-NH_3, H_3B-PH_3, H_3Al-NH_3 and H_3Al-PH_3) where the extent of charge transfer (CT) varies. In this Article we perform a detailed quantum chemical analysis on these systems. We have quantified the extent of CT in these systems based on the separation of the total energy into various components [nuclear−nuclear potential energy (V_{nn}), electron−nuclear potential energy (V_{en}), electron−electron potential energy (V_{ee}) and kinetic energy (KE)]. We discuss the role of back-bonding that sets in due to CT in these systems and thus affects the rotational barrier. We also study the change in conformational preference in such EDA systems on introducing a conjugative spacer between the donor and the acceptor groups. For such systems, the preference for a staggered or eclipsed orientation depends critically on the number of nodes in the wave functions.

2. Computational Details

All the calculations were carried out using the Gaussian 03 set of programs.[17] The structures of the molecules were optimized using the Møller−Plesset(MP2)[18] and DFT based B3LYP method at the 6-31++G(d,p) basis set level.[18] Frequency analysis was additionally performed for the optimized geometries and no imaginary frequencies were found. The staggered conformer corresponds to a dihedral twist (ϕ) of 60° or 180° about the central X−Y bond, whereas the eclipsed conformer has a dihedral twist of 0° or 120°. Our computational analysis involves spanning the conformational space from the optimized staggered geometry to the eclipsed geometry with an increment of 10° in ϕ keeping all the other structural parameters in the molecule unchanged. Spanning the conformation space by a rigid rotation about the central X−Y bond is a valid assumption; as this does not significantly perturb the energies of the rigid-rotated conformers, we find that the energy difference between the optimized and the rigid-rotated conformers is negligible when compared with the magnitude of the rotational barriers (see Supporting Information). For the conjugative spacers acetylene and benzene, the rotational barriers are reported as energy differences between optimized geometries of the eclipsed and staggered conformers. No rigid rotation has been assumed for these conjugative spacers due to the low values of the rotational barrier.

3. Results and Discussions

We define the rotational barrier as the difference in the total energy between the eclipsed and the staggered conformer. We find that, compared to homonuclear systems where an increase in the X−X distance invariably decreases the rotational barrier, the CT systems behave distinctly in a different way. For H_3B-

* Corresponding author. E-mail: pati@jncasr.ac.in.

10.1021/jp0575761 CCC: $33.50
Published on Web 03/25/2006

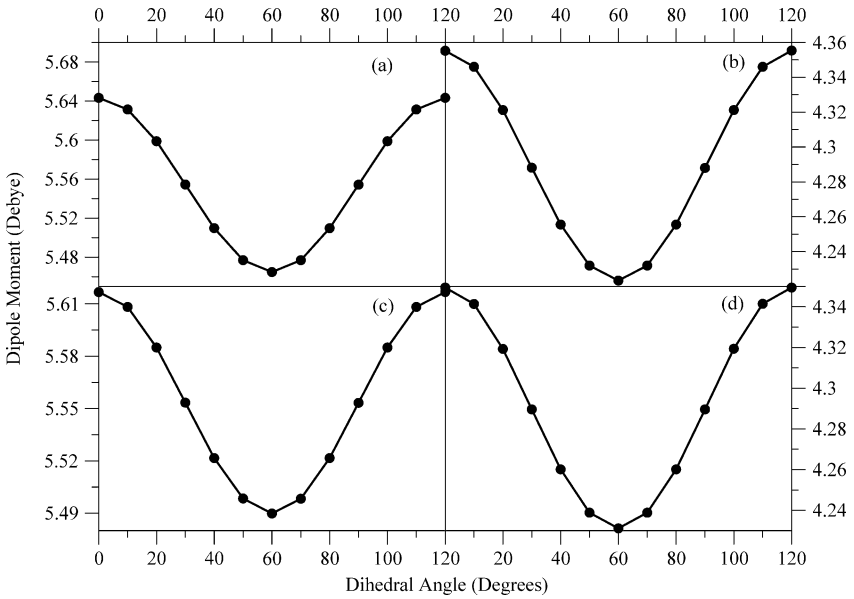

Figure 1. Variation in dipole moment as a function of the dihedral angle for (a) H_3B-NH_3, (b) H_3B-PH_3, (c) H_3Al-NH_3 and (d) H_3Al-PH_3. Dipole moments are reported in Debye and dihedral angles in degrees.

NH_3, H_3B-PH_3, H_3Al-NH_3 and H_3Al-PH_3 the computed rotational barriers are 2.48 kcal/mol (2.62 kcal/mol), 2.47 kcal/mol (2.55 kcal/mol), 0.69 kcal/mol (0.84 kcal/mol) and 0.95 kcal/mol (0.97 kcal/mol), respectively. The values in parentheses correspond to rotational barriers calculated at the MP2 level. Positive energy values indicate destabilization of the eclipsed conformation with respect to the staggered conformation. As can be seen, for the boron analogues, the rotational barrier decreases by 0.01 kcal/mol for an increase in the internuclear X−Y distance by 0.29 Å from 1.66 Å (H_3B-NH_3) to 1.95 Å (H_3B-PH_3) (a decrease of 0.07 kcal/mol verified at the MP2 level). For the aluminum analogues, however, the rotational barrier increases (instead of decreasing) by 0.24 kcal/mol as the X−Y distance increases from 2.09 Å (H_3Al-NH_3) to 2.58 Å (H_3Al-PH_3), an increase of 0.49 Å (an increase of 0.13 kcal/mol is verified at the MP2 level). Interestingly, such an increase (0.82 Å) in the central bond distance for the isoelectronic systems that do not exhibit charge transfer from H_3C-CH_3 (1.53 Å) to $H_3Si-SiH_3$ (2.35 Å) causes a decrease in the rotational barrier by 1.9 kcal/mol.

The anomalous behavior of the rotational barrier in these EDA systems cannot be explained by a simple steric interactions model as it would invariably lead to a decrease in rotational barrier with increase in the X−Y bond length. We find that it is the effective CT for these systems and "back bonding" effect for H_3B-PH_3 and H_3Al-PH_3 that quantitatively describe the rotational barrier in these systems and govern the conformational preference.

3.1. Charge Transfer. EDA systems are associated with CT and thereby a definite dipole moment. We find that the dipole moment varies with the dihedral angle and is largest for the eclipsed conformer and lowest for the staggered conformer (Figure 1). The fact that dipole moment changes with the dihedral angle suggests the presence of different CT interactions in the staggered and eclipsed conformations. The dipole moment for these molecules decreases in the order: H_3B-NH_3 (5.64 D) ≈ H_3Al-NH_3 (5.62 D) > H_3Al-PH_3 (4.36 D) ≈ H_3B-PH_3 (4.35 D). Note that we report only the dipole moment for the eclipsed conformer in the parentheses.

We have analyzed the Mulliken charge population and natural population analysis (NPA) for all of these systems to quantify the amount of CT between the fragments (from NH_3, PH_3 to BH_3, AlH_3 respectively). The results of the Mulliken population analysis and NPA are summarized in Table 1. The extent of CT between the fragments follows the order H_3B-PH_3 > H_3B-NH_3 > H_3Al-PH_3 > H_3Al-NH_3. Such a CT profile can be explained by hard soft acid base principle (HSAB).[19] According to the HSAB principle, hard acids bind with hard bases and soft acids bind with soft bases. The η (absolute hardness) values of Al, B, P, and N are 2.77, 4.01, 4.88, and 7.23 eV, respectively.[20] These values clearly indicate that the formation of H_3B-PH_3 is more favorable (soft acid−soft base) than formation of H_3B-NH_3 (soft acid−hard base). The formation of H_3Al-PH_3 and H_3Al-NH_3 is unfavorable in comparison with the boron analogue formation. From the Mulliken charge analysis and NPA(values in parentheses), we find that the charge on BH_3 decreases substantially from H_3B-PH_3 −0.46e (−0.59e) to H_3B-NH_3 −0.31e (−0.35e), a decrease of 0.15e (0.25e). On the other hand, the charge on AlH_3 remains almost unchanged from H_3Al-PH_3 −0.26e (−0.23e) to H_3Al-NH_3 −0.24e (−0.16), a decrease of only 0.02e (0.07e). Therefore, both the charge analysis and HSAB principle explain the boron analogues to be better acceptors compared to aluminum analogues. In Figure 2a,b we plot the HOMO−LUMO energies for BH_3, NH_3, AlH_3 and BH_3, PH_3, AlH_3 respectively. We find that the HOMO−LUMO picture supports the charge transfer and HSAB analysis; the HOMO(NH_3)−LUMO(BH_3) and HOMO(PH_3)−LUMO(BH_3) gaps, 4.62 and 4.52 eV respectively, are smaller compared to the HOMO(NH_3)−LUMO(AlH_3) and HOMO(PH_3)−LUMO(AlH_3) gaps, 5.00 eV and 4.96, respectively. This clearly indicates that BH_3 is a better acceptor compared to AlH_3.

TABLE 1: Mulliken Population Analysis and Natural Population Analysis (NPA) for H_3X-YH_3 (X = B, Al; Y = N, P) Systems[a]

analysis type	H_3B-NH_3		H_3B-PH_3		H_3Al-NH_3		H_3Al-PH_3	
	$-BH_3$	$-NH_3$	$-BH_3$	$-PH_3$	$-AlH_3$	$-NH_3$	$-AlH_3$	$-PH_3$
Mulliken	−0.309	0.309	−0.464	0.464	−0.243	0.243	−0.258	0.258
NPA	−0.352	0.352	−0.590	0.590	−0.157	0.157	−0.232	0.232

[a] Charges are reported in electronic units.

3.2. Symmetry of the Molecular Orbitals. To identify the dominant contributions to the conformational preference, we

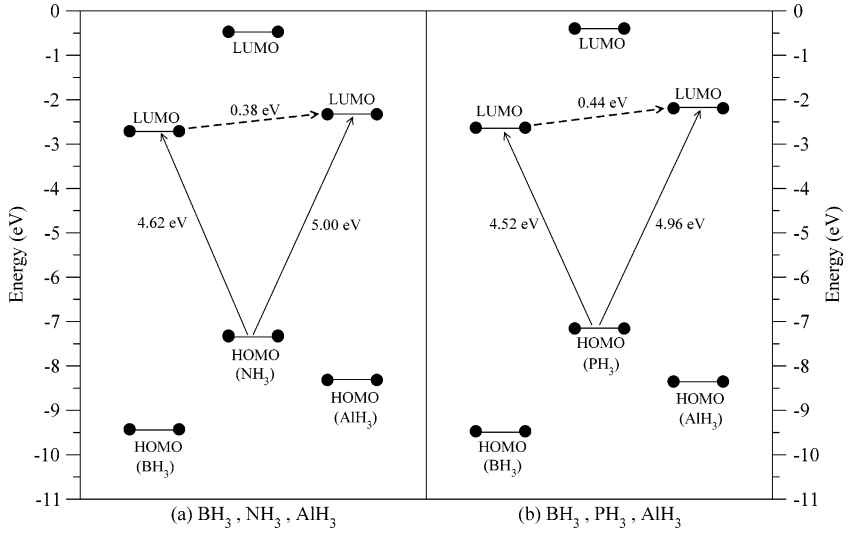

Figure 2. HOMO−LUMO gaps for (a) BH_3, NH_3, AlH_3 and (b) BH_3, PH_3, AlH_3. Energies are reported in electronvolts.

TABLE 2: Symmetry of the Orbitals for H_3X-YH_3 (X = B, Al; Y = N, P) Systems and Contributions of V_{en} to the HOMO, HOMO−1, HOMO−2 and HOMO−3 for Staggered and Eclipsed Conformers and Contributions of V_{ee} and KE for the Same[a]

(a) Symmetry and V_{en} Contributions

	HOMO		HOMO−1		HOMO−2		HOMO−3	
molecule	S	V_{en}	S	V_{en}	S	V_{en}	S	V_{en}
H_3B-NH_3ec	E	−6.524	A	−8.071	A	−8.787	E	−9.150
H_3B-NH_3st	E	−6.512	A1	−8.089	A1	−8.769	E	−9.155
H_3B-PH_3ec	E	−8.082	A	−10.424	E	−10.349	A	−9.823
H_3B-PH_3st	E	−8.077	A1	−10.442	E	−10.353	A1	−9.082
H_3Al-NH_3ec	E	−8.030	A1	−9.581	A1	−11.086	E	−10.603
H_3Al-NH_3st	E	−8.024	A1	−9.591	A1	−11.078	E	−10.603
H_3Al-PH_3ec	E	−9.187	A1	−11.885	A1	−11.390	E	−11.414
H_3Al-PH_3st	E	−9.184	A1	−11.905	A1	−11.368	E	−11.412

(b) V_{ee} Contributions and KE

	HOMO		HOMO−1		HOMO−2		HOMO−3	
molecule	V_{ee}	KE	V_{ee}	KE	V_{ee}	KE	V_{ee}	KE
H_3B-NH_3ec	5.521	0.727	6.507	1.206	7.060	1.212	7.246	1.347
H_3B-NH_3st	5.513	0.720	6.521	1.210	7.046	1.209	7.250	1.350
H_3B-PH_3ec	7.076	0.703	8.834	1.267	8.820	1.083	8.304	1.016
H_3B-PH_3st	7.072	0.699	8.851	1.268	8.823	1.085	8.283	1.013
H_3Al-NH_3ec	7.083	0.681	8.146	1.097	9.329	1.311	8.700	1.350
H_3Al-NH_3st	7.080	0.677	8.152	1.100	9.324	1.309	8.699	1.351
H_3Al-PH_3ec	8.228	0.679	10.309	1.257	10.003	0.966	9.879	1.091
H_3Al-PH_3st	8.227	0.677	10.327	1.260	9.984	0.963	9.878	1.091

[a] Code: st, staggered, ec, eclipsed, S, symmetry, V_{en}, electron−nuclear potential energy, V_{ee}, electron−electron potential energy, KE, kinetic energy. Energies are reported in kcal/mol.

utilize a fragmentation scheme[21] to separate the occupied molecular orbitals into σ and π types. In this fragmentation scheme, each of the H_3 fragment consists of three hydrogen atoms of the $-XH_3$, $-YH_3$ groups. Linear combination of the 1s atomic orbitals of the three hydrogens gives rise to three molecular orbitals (MO): one σ type and two π type orbitals. Terming the three hydrogens in a H_3 as a, b and c, we can write the MOs as shown in eq 1 with a trivial normalization constant for

$$\sigma = [1s_a + 1s_b + 1s_c]$$
$$\pi = [1s_a - (1/2)1s_b - (1/2)1s_c]$$
$$\pi' = [1s_b - 1s_c] \quad (1)$$

each molecular orbital. The σ orbital is a symmetric combination

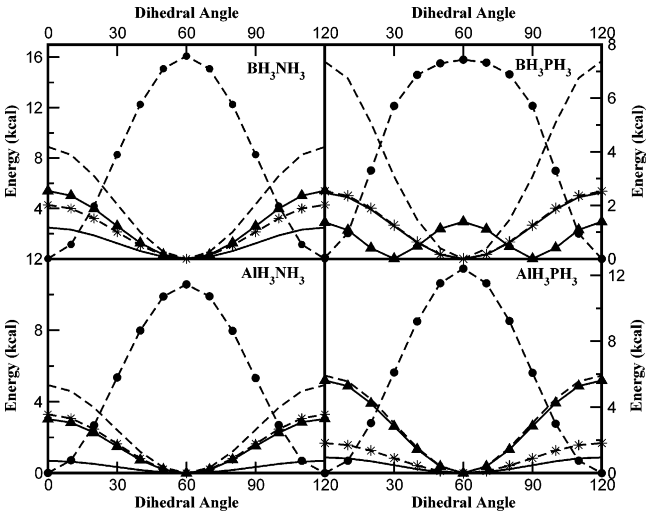

Figure 3. Variation in conformational energy as a function of the dihedral angle for H_3B-NH_3, H_3B-PH_3, H_3Al-NH_3 and H_3Al-PH_3. The energy of the staggered form is scaled to zero and the *Y*-axis corresponds to destabilization. Code: dashed line with filled circle, V_{en}; straight line with triangle, V_{ee}; dashed line with no symbol, kinetic energy; dashed line with star, V_{nn}; straight line with no symbol, total energy. Energies are reported in kcal/mol and dihedral angles in degrees.

whereas the π orbitals have phase difference in different lobes. The p_y and p_x orbitals in the X−Y fragment (along the *z*-axis) interact with the π and π' orbitals, respectively, and are thus associated with the π bonding. The interaction of the p_z orbital in the X−Y fragment with the σ orbital of H_3 is associated with the σ backbone. Using this fragmentation scheme, we try to investigate the dominant contributions from the π and the σ backbone.

An analysis of the symmetries of the frontier molecular orbitals [HOMO, HOMO−1, HOMO−2 and HOMO−3] for the staggered and the eclipsed conformers have been performed for all the four molecular systems. Table 2 shows the symmetry characteristics of these levels. For H_3B-NH_3, the HOMO and HOMO−3 have E symmetry and HOMO−1 and HOMO−2 have A type symmetry. In H_3B-PH_3, HOMO and HOMO−2 are E type and HOMO−1 and HOMO−3 are A type. In H_3Al-NH_3 and H_3Al-PH_3, the HOMO and HOMO−3 are E type whereas the HOMO−1 and HOMO−2 are distinctly A type. Very interestingly, we find that the molecular orbital coefficients for the A type and the degenerate E type orbitals for all the

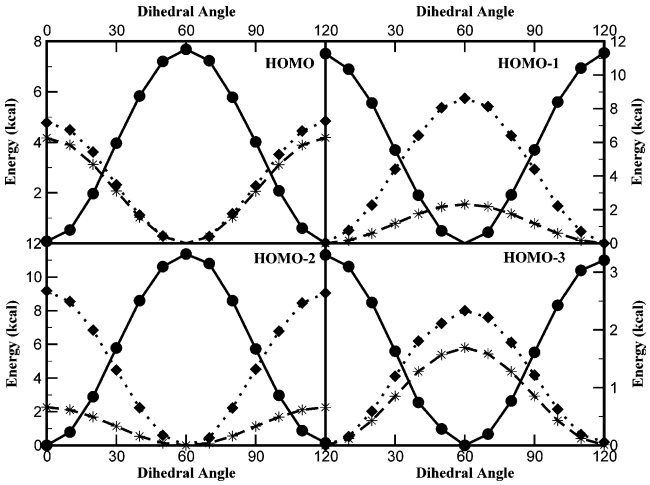

Figure 4. Individual contributions of V_{en}, V_{ee} and kinetic energy to HOMO [E], HOMO−1 [A], HOMO−2 [A], and HOMO−3 [E] levels for H_3B-NH_3 (scaled to show the amount of destabilization). Note that HOMO and HOMO−3 pairs are degenerate. Code: straight (circles), V_{en}; dotted (square), V_{ee}; dashed (star), kinetic energy. Energies are reported in kcal/mol and dihedral angles in degrees.

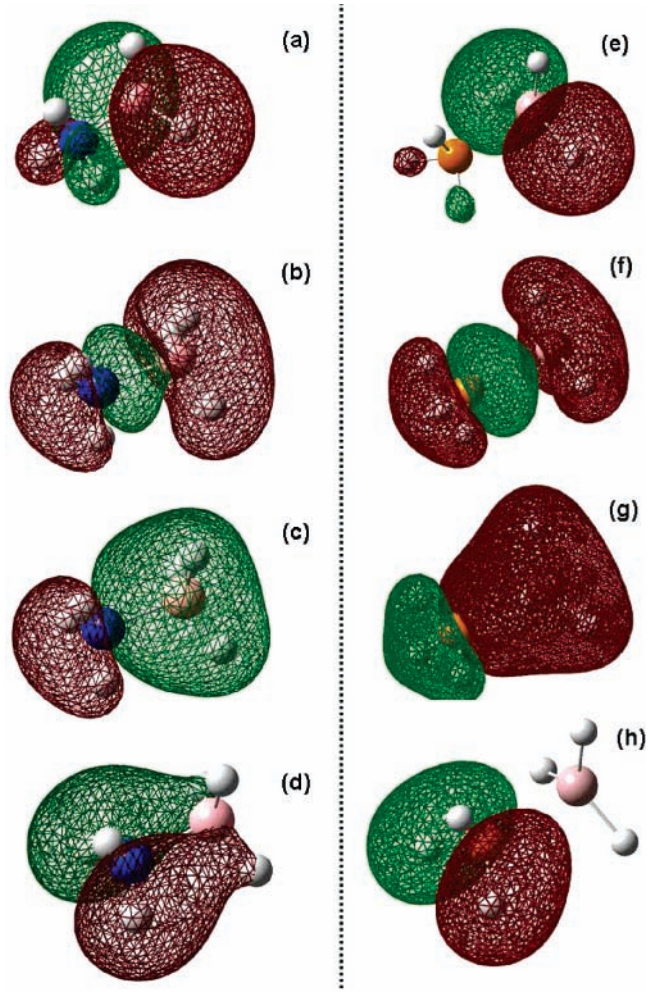

Figure 5. Wave function plots for H_3B-NH_3 and H_3Al-PH_3 for HOMO (a) and (e) and HOMO−1 (b) and (f) showing CT from $NH_3 \rightarrow BH_3$ and $PH_3 \rightarrow AlH_3$ respectively. HOMO−2 (c) and (g) and HOMO−3 (d) and (h) showing CT from $BH_3 \rightarrow NH_3$ and $AlH_3 \rightarrow PH_3$ respectively.

systems resembles the σ and the two π type orbitals (see eq 1), respectively.

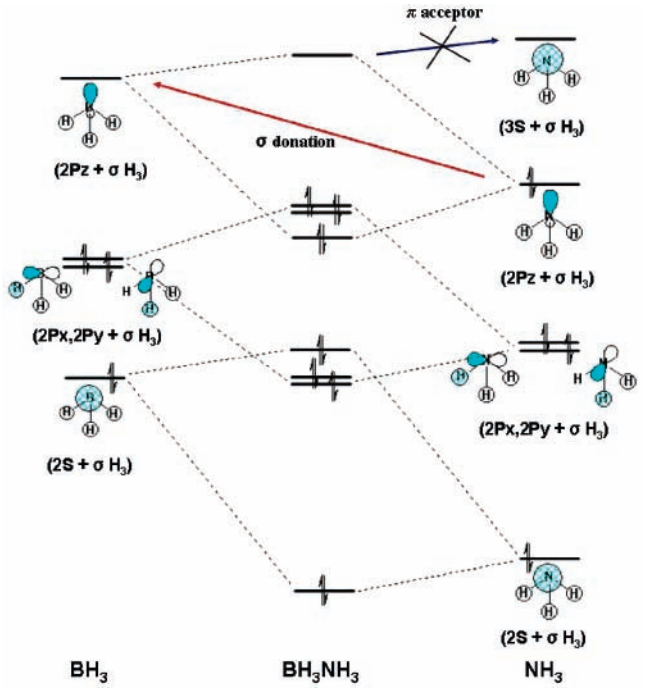

Figure 6. Molecular orbital correlation diagram for H_3B-NH_3. The NH_3 ligand acts as a σ donor but cannot act as π acceptor.

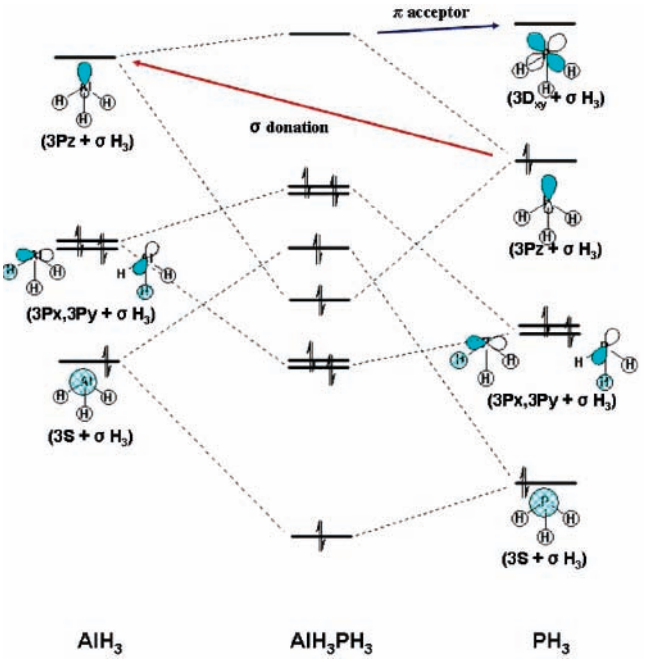

Figure 7. Molecular orbital correlation diagram for H_3Al-PH_3. The PH_3 ligand acts as a σ donor as well as a π acceptor.

3.3. Energy Decomposition. For a quantitative analysis of the conformational stability, the total energy ($E_{tot.}$) is separated into various contributions as $E_{tot.} = KE + V_{ee} + V_{en} + V_{nn}$.[22] KE is kinetic energy, V_{ee} is electron−electron potential energy, V_{en} is electron−nuclear potential energy and V_{nn} is nuclear−nuclear potential energy. The plot of the total energy and the contributions from each term for all the systems is shown in Figure 3. As can be seen, the electron−nuclear potential energy, V_{en}, destabilizes the staggered conformation whereas all other components (V_{ee}, V_{nn} and KE) stabilize the staggered conformation for all the systems.

For H_3B-NH_3, the eclipsed to staggered rotation involves $E_{tot.} = 2.48$ kcal/mol, $V_{en} = -16.09$ kcal/mol, $V_{ee} =$

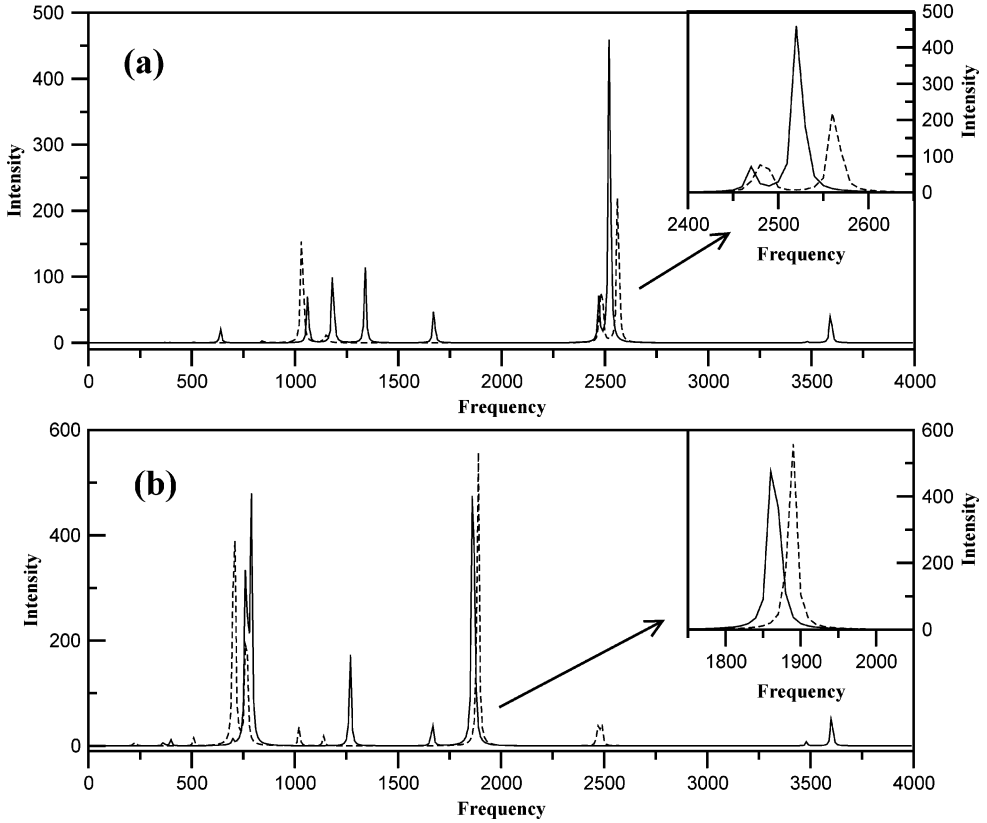

Figure 8. IR spectrum: (a) H_3B-NH_3 and H_3B-PH_3; (b) H_3Al-NH_3 and H_3Al-PH_3. Inset: metal−H stretching frequencies. Legend: (a) black (solid line), H_3B-NH_3; black (dotted line), H_3B-PH_3; (b) black (solid line), H_3Al-NH_3; black (dotted line): H_3Al-PH_3. Frequency are reported in cm^{-1}.

5.40 kcal/mol, V_{nn} = 4.28 kcal/mol and KE = 8.88 kcal/mol. Positive energies indicate destabilization of the eclipsed conformer with respect to the staggered conformer. For H_3B-PH_3, a similar dihedral angle twist involves $E_{tot.}$ = 2.47 kcal/mol, V_{en} = −7.43 kcal/mol, V_{ee} = 1.38 kcal/mol, V_{nn} = 2.52 kcal/mol and KE = 7.38 kcal/mol. For H_3Al-NH_3, $E_{tot.}$ = 0.69 kcal/mol, V_{en} = −10.56 kcal/mol, V_{ee} = 3.03 kcal/mol, V_{nn} = 3.29 kcal/mol and KE = 4.93 kcal/mol. For H_3Al-PH_3, $E_{tot.}$ = 0.95 kcal/mol, V_{en} = −12.40 kcal/mol, V_{ee} = 5.61 kcal/mol, V_{nn} = 1.82 kcal/mol and KE = 5.91 kcal/mol. In Table 2, we report the contributions of KE, V_{ee}, and V_{en} for the eclipsed and the staggered conformations for all the systems corresponding to each molecular orbital from HOMO to HOMO−3, the contributions are calculated as $\langle MO|KE|MO\rangle$, $\langle MO|V_{ee}|MO\rangle$, $\langle MO|V_{en}|MO\rangle$ and $\langle MO|V_{nn}|MO\rangle$, respectively, where MO corresponds to the molecular orbital being studied. Figure 4 shows the variation of KE, V_{ee} and V_{en} with respect to the dihedral angle for HOMO, HOMO−1, HOMO−2 and HOMO−3 for H_3B-NH_3. It is clear that V_{ee} and KE terms stabilize the staggered conformer in HOMO and HOMO−2, which are E type and A type orbitals, respectively. On the other hand, for HOMO−1 and HOMO−3, which are A and E type orbitals, respectively, V_{ee} and KE terms destabilize the staggered conformer, the main point is that the CT characteristic of the orbital is as important as the symmetry of the orbital (see Supporting Information file for similar plots for other three systems).

We analyze the plots of the wave functions (Figure 5) and classify the CT associated with each frontier orbital (HOMO, HOMO−1, HOMO−2, and HOMO−3). For the systems under consideration, the HOMO and HOMO−1 show CT from NH_3, PH_3 to BH_3, AlH_3 (N, P → B, Al) whereas the HOMO−2 and HOMO−3 show CT from BH_3, AlH_3 to NH_3, PH_3 (B, Al → N, P). Using the fragmentation scheme described earlier (eq 1), we identify the corresponding σ and the π type orbitals. In H_3B-NH_3, H_3Al-NH_3 and H_3Al-PH_3, the HOMO and HOMO−3 are degenerate π type orbitals and the HOMO−1, HOMO−2 are the σ type orbitals. In H_3B-PH_3, the HOMO and HOMO−2 are degenerate π type of orbitals whereas the HOMO−1, HOMO−3 are of σ type.

The stabilization of the staggered conformer for each system is analyzed by separating out the contributions made by the various energy components to the π and the σ orbitals. We then find the orbital governing the conformational preference. It is noted that the orbitals that have a stabilizing contribution from V_{ee} and KE always have a destabilizing contribution by V_{en}. Note that the positive energy values indicate the stabilization of the staggered conformer compared to the eclipsed conformer and the negative energy values indicate the destabilization of the staggered conformer compared to the eclipsed conformer.

The contributions from these energy components to the π type and σ type orbitals is analyzed for the four systems. We define Δ as the sum or difference in the energy components (V_{ee}, V_{en} and KE) for each system keeping in mind the fact that the Δ, thus defined, stabilizes the staggered conformation.

(i) H_3B-NH_3:

π contributions: $\Delta = E_{HOMO} - E_{HOMO-3}$

ΔV_{ee} = 2.44 kcal/mol; ΔV_{en} = −4.38 kcal/mol; ΔKE = 2.48 kcal/mol

σ contributions: $\Delta = E_{HOMO-1} - E_{HOMO-2}$

ΔV_{ee} = 0.55 kcal/mol; ΔV_{en} = −0.08 kcal/mol; ΔKE = −0.05 kcal/mol

It is clear that the magnitude of the contributions stabilizing the staggered conformation is greater for the π orbitals when compared to the σ orbital. This is to say that for H_3B-NH_3, CT is governed by the π(HOMO) orbital, which has a N → B CT profile.

(ii) H_3B-PH_3:

π **contributions**: $\Delta = E_{HOMO} - E_{HOMO-2}$

$\Delta V_{ee} = 0.34$ kcal/mol; $\Delta V_{en} = -0.87$ kcal/mol; $\Delta KE = 1.79$ kcal/mol

σ **contributions**: $\Delta = E_{HOMO-3} - E_{HOMO-1}$

$\Delta V_{ee} = 2.60$ kcal/mol; $\Delta V_{en} = -3.24$ kcal/mol; $\Delta KE = 0.85$ kcal/mol

Using the same parameter as for H_3B-NH_3, we find that for H_3B-PH_3, the dominant contribution is from the σ(HOMO−3) orbital. Apart from that, H_3B-PH_3 also has marginal contribution from the π(HOMO) orbital. Although the σ-(HOMO−3) orbital has a B → P CT characteristic, π(HOMO) has a P → B CT characteristic. The involvement of the σ orbital-(B → P CT orbital) in controlling the geometry is indicative of back bonding due to the involvement of the vacant d-orbitals of phosphorus.

(iii) H_3Al-NH_3:

π **contributions**: $\Delta = E_{HOMO} + E_{HOMO-3}$. We have defined Δ as a sum because both the orbitals stabilize the staggered conformer

$\Delta V_{ee} = 2.09$ kcal/mol; $\Delta V_{en} = -3.72$ kcal/mol; $\Delta KE = 1.82$ kcal/mol

σ **contributions**: $\Delta = E_{HOMO-1} - E_{HOMO-2}$

$\Delta V_{ee} = -0.99$ kcal/mol; $\Delta V_{en} = 1.33$ kcal/mol; $\Delta KE = -0.53$ kcal/mol

We note that for H_3Al-NH_3, the dominant stable contribution is from the π(HOMO). Also, there exists a destabilizing dominant contribution from σ(HOMO−1) orbitals. Note that both the orbitals show N → Al CT. The π orbitals stabilize the staggered conformer, whereas the σ orbital destabilizes the staggered conformer. These two effects being of opposite character lead to the overall reduction of the rotational barrier.

(iv) H_3Al-PH_3:

π **contributions**: $\Delta = E_{HOMO} + E_{HOMO-3}$. As in H_3Al-NH_3, we define Δ as a sum because both orbitals stabilize the staggered conformer.

$\Delta V_{ee} = 1.79$ kcal/mol; $\Delta V_{en} = -2.76$ kcal/mol; $\Delta KE = 1.61$ kcal/mol

σ contributions: $\Delta = E_{HOMO-2} - E_{HOMO-1}$

$\Delta V_{ee} = 0.47$ kcal/mol, $\Delta V_{en} = -1.41$ kcal/mol, $\Delta KE = -0.30$ kcal/mol

In this case both the π(HOMO) (P → Al CT orbital) and the σ(HOMO−2) (Al → P CT orbital) orbitals have dominant contribution and stabilize the staggered conformer. As a result, the rotational barrier increases. The involvement of the σ orbitals in stabilizing the staggered conformer as in the case of H_3B-PH_3 again indicates the presence of back bonding.

It is to be noted that the analysis of the stability of the staggered conformation in the light of the dominant contributions from the π and the σ type of orbitals brings out the salient features of the rotational barrier and back bonding. We provide further proof of back bonding by performing a molecular orbital correlation analysis.

3.4. Molecular Orbital Correlation Analysis. We perform MO correlation analysis to quantify the σ donor ability and π acceptor ability of the ligands, NH_3 and PH_3. We have plotted the MO correlation diagram for boron analogues and aluminum analogues in Figures 6 and 7, respectively. Note that both NH_3 and PH_3 are good σ donors; however, only PH_3 behaves as a π acceptor due to the low lying antibonding d-orbitals, which are favorable for accepting the B, Al → P back-donation of the electrons.[23,24] For all the systems, the σ donation (N, P → B, Al) is from the hybrid orbital formed between p_z orbital of N, P and σ orbital of H_3 as defined in eq 1. The formation of such hybrid orbitals is reported in the literature.[25,26] For H_3B-NH_3 and H_3Al-NH_3, there are no favorable antibonding orbitals in N to accept the B, Al → N back-donation of the electrons and thus there is no back bonding in these systems.

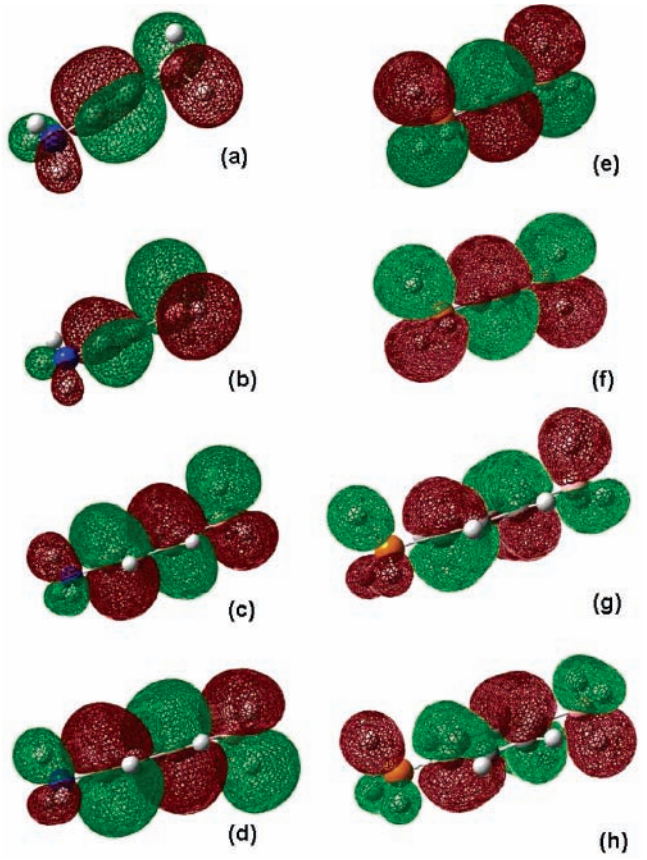

Figure 9. Wave function plots (HOMO) for CT systems with a conjugative spacer between them for (a) H_3B-acetylene$-NH_3$-(eclipsed), (b) H_3B-acetylene$-NH_3$(staggered), (c) H_3B-benzene$-NH_3$(eclipsed), (d) H_3B-benzene$-NH_3$(staggered), (e) H_3B-acetylene$-PH_3$(eclipsed), (f) H_3B-acetylene$-PH_3$(staggered), (g) H_3B-benzene$-PH_3$(eclipsed) and (h) H_3B-benzene$-PH_3$(staggered).

We have also calculated the infrared spectrum (IR) for these systems. They are plotted in Figure 8 for all the four cases to verify the presence of back bonding in H_3B-PH_3 and H_3Al-PH_3. As can be seen, the IR stretching frequency of the B−H bond increases in magnitude by 40.7 cm^{-1} from H_3B-NH_3 to H_3B-PH_3. Similarly, for the Al−H bond, the stretching frequency increases by 23.7 cm^{-1} from H_3Al-NH_3 to H_3Al-PH_3. This increase in the IR stretching frequency is due to the back-donation of electrons from B, Al → P, these electrons are involved in π bonding, which effectively reduces the electron density on the metal[23] and shortens the (B, Al)−H bond. Such effects are clearly missing in H_3B-NH_3 and H_3Al-NH_3.

3.5. Conjugative Spacer. The changes in conformational preferences on introduction of conjugative spacers between the donor and the acceptor groups have been studied by introducing two conjugative spacers (acetylene and benzene) between the donor and the acceptor groups.

Acetylene Spacer. On performing a geometry optimization for H_3X-acetylene$-YH_3$ (X = B, Al; Y = N, P), we find the stable structure to be eclipsed and not staggered. Frequency analysis reveals that the staggered conformer has one imaginary frequency associated with the torsional bending to the more favored eclipsed conformer. An optimization at the MP2 level shows that the C3 symmetry is broken due to local distortion

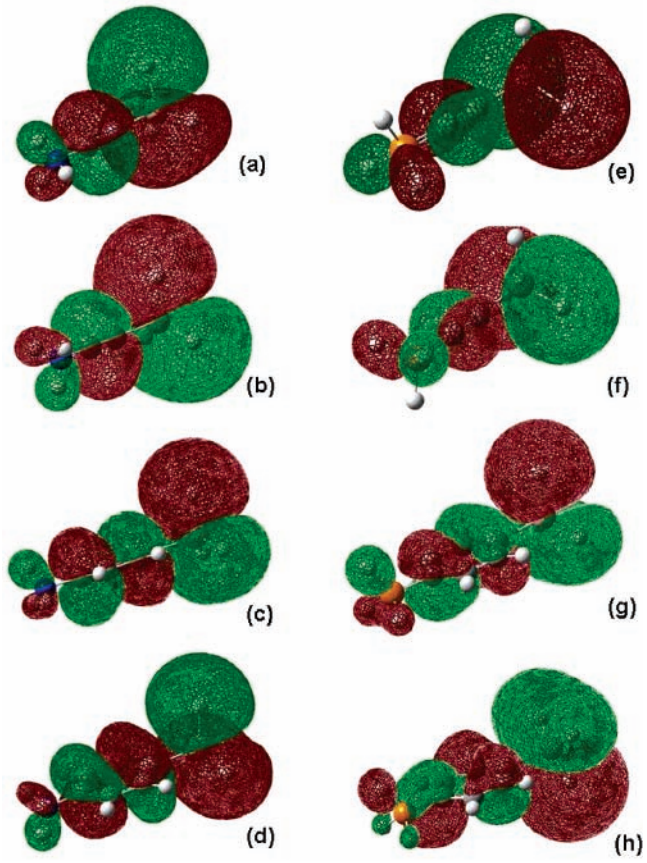

Figure 10. Wave function plots (HOMO) for CT systems with a conjugative spacer between them for (a) $H_3Al-acetylene-NH_3$(eclipsed), (b) $H_3Al-acetylene-NH_3$(staggered), (c) $H_3Al-benzene-NH_3$(eclipsed), (d) $H_3Al-benzene-NH_3$(staggered), (e) $H_3Al-acetylene-PH_3$(eclipsed), (f) $H_3Al-acetylene-PH_3$(staggered), (g) $H_3Al-benzene-PH_3$(eclipsed) and (h) $H_3Al-benzene-PH_3$(staggered).

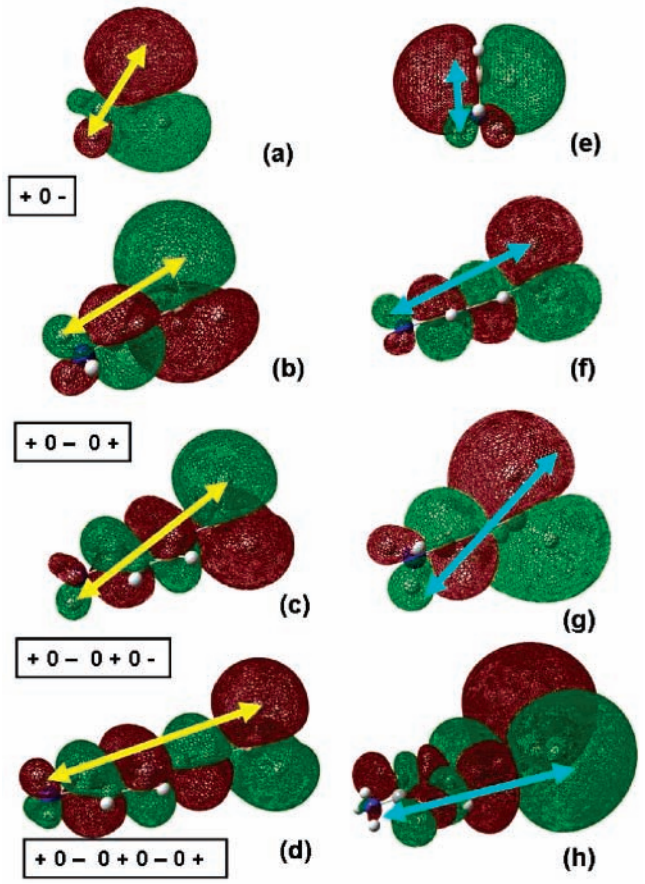

Figure 11. In-phase and out-of-phase combination of the donor−acceptor orbitals for H_3Al-NH_3 and its analogues: (a) H_3N-AlH_3-(staggered), (b) $H_3N-acetylene-AlH_3$(eclipsed), (c) $H_3N-benzene-AlH_3$(staggered), (d) $H_3N-benzene-acetylene-AlH_3$(eclipsed), (e) H_3N-AlH_3(eclipsed), (f) $H_3N-benzene-AlH_3$(eclipsed), (g) $H_3N-acetylene-AlH_3$(staggered) and (h) $H_3N-benzene-acetylene-AlH_3$-(staggered). Color code: green lobe, positive wave function(+); red lobe, negative wave function(−); yellow arrow, in-phase combination; blue arrow, out-of-phase combination. Box: Combination of the nodes.

in the acetylene spacer. Though the C3 symmetry is lost at the MP2 level, the eclipsed and staggered nature of the conformers is still maintained (see Supporting Information file for the optimized structures at MP2 level). The rotational barriers for the system under consideration are found to be −0.055 kcal/mol (−0.063 kcal/mol), −0.029 kcal/mol (−0.032 kcal/mol), −0.041 kcal/mol (−0.040 kcal/mol) and −0.019 kcal/mol (−0.008 kcal/mol) for $H_3B-acetylene-NH_3$, $H_3B-acetylene-PH_3$, $H_3Al-acetylene-NH_3$, and $H_3Al-acetylene-PH_3$, respectively; values in parentheses correspond to rotational barriers calculated at the MP2 level. The negative value of the rotational barrier implies that the eclipsed conformer is more stable compared to the staggered conformer. Such a result is counterintuitive, because increasing the distances between the donor and the acceptor groups should decrease the rotational barrier as naively can be expected.

However, the fact that the conformational preference shifts from staggered to eclipsed conformer suggests the presence of specific electronic interactions between the donor−acceptor groups at either ends through the acetylene spacer. In Figures 9 and 10, we plot the HOMO wave function for the staggered and the eclipsed conformers for all the systems. One clearly observes an in-phase combination of the donor−acceptor orbitals in the eclipsed conformer (Figures 9a and 10a and Figures 9e and 10e) and an out-of-phase combination in the staggered conformation (Figures 9b and 10b and Figures 9f and 10f), supporting our conclusion of extended electronic conjugation through the acetylene unit in the eclipsed form. Thus, the acetylene unit acts as a conjugation "relay" between the donor−acceptor groups.

Benzene Spacer. When the geometry of the $H_3X-benzene-YH_3$ (X = B, Al; Y = N, P) systems is optimized, the staggered conformer is found to be more stable compared to the eclipsed conformer, no distortion of the C_3 symmetry is observed at the B3LYP and MP2 level of optimization. The rotational barriers are calculated as 0.36 kcal/mol (0.40 kcal/mol), 0.31 kcal/mol (0.35 kcal/mol), 0.25 kcal/mol (0.34 kcal/mol) and 0.51 kcal/mol (0.56 kcal/mol) for $H_3B-benzene-NH_3$, $H_3B-benzene-PH_3$, $H_3Al-benzene-NH_3$ and $H_3Al-benzene-PH_3$, respectively, the values in the parentheses correspond to rotational barriers calculated at the MP2 level. This change in the conformational preference from the eclipsed (for an acetylene spacer) to staggered (for a benzene spacer) conformer can be understood by analyzing number of nodes between the donor and the acceptor groups. We find that the number of nodes between the donor and the acceptor groups controls the conformational preference. For odd numbers of nodes (H_3X-YH_3, $H_3X-benzene-YH_3$) the staggered conformer is the preferred geometry whereas for even numbers of nodes ($H_3X-acetylene-YH_3$), the eclipsed conformer is the preferred geometry.

We find that an in-phase combination of orbitals stabilizes a conformer whereas an out-of-phase combination of the orbitals

destabilizes a conformer. We plot the variations in the conformational preference with the number of nodes in Figure 11. The yellow arrows indicate an in-phase combination of the donor−acceptor orbitals and the blue arrows indicate an out-of-phase combination of the donor−acceptor orbitals. We denote a positive lobe as (+), a negative lobe as (−) and a node as (0). We find that for a system with odd number of nodes, the combination goes as +0− and +0−0+0−. Thus, at the two ends, the sign of the wave function remains opposite, which corresponds to a staggered geometry. However, for systems with even number of nodes, the combination +0−0+ and +0−0+0−0+, suggests that the sign of the wave function does not change at the two ends, corresponding to a eclipsed geometry.

To strengthen our analysis, we further optimize a system with four nodes (H_3X−benzene−acetylene−YH_3) and find the stable conformer to be eclipsed (Figure 11d). This observation confirms our statement that the number of nodes controls the conformational geometry of an extended system.

4. Conclusions

On the basis of our detailed analysis of the rotational barriers for the CT heteroatomic (isoelectronic) ethane congeners, we find that the rotational barrier in these systems depends crucially on the CT efficiency from the donor to the acceptor. The insensitivity of the change in rotational barrier to increase in the X−Y distances from B−N to B−P and decrease in the rotational barrier with increase in the X−Y distances from Al−N to Al−P arises due to the dominant presence of back bonding from BH_3(AlH_3) to the PH_3 that is absent for BH_3−NH_3 and AlH_3−NH_3. The decomposition of the energies into the σ and π orbital interactions and IR stretching frequencies of B−H and Al−H quantitatively explains such changes. Dependence of the conformational preference on the in-phase and out-of-phase combination of the donor−acceptor orbitals is investigated. Such a detailed investigation for the rotational barriers in the CT systems have a potential application in understanding the structure and property relations in biopolymers and self-assembled monolayers and also molecular electronic properties of small CT molecules. We note that the effective conjugation between donor/acceptor systems connected by conjugative unit (like acetylene and benzene) is quite a well-known phenomenon,[27] but the fact that a CT phenomenon reverses the conformational preference in such molecular systems is novel and may have implications in future device integration at the molecular scale.

Acknowledgment. S.S.M. and A.D. thank CSIR for the JR and SR fellowships, respectively. S.K.P. acknowledges CSIR and DST, Government of India, for the research grants.

Supporting Information Available: Energy differences between optimized and the rigid-rotated conformers for all systems. Individual contributions of V_{en}, V_{ee} and kinetic energy to frontier orbitals of H_3B−PH_3, H_3Al−NH_3, and H_3Al−PH_3. Optimized geometries of the CT systems with an acetylene spacer. Complete citation of ref 17. This material is available free of charge via Internet at http://pubs.acs.org.

References and Notes

(1) Eliel, E. L. *Stereochemistry of Carbon Compounds*; McGraw-Hill Inc.: New York, 1962.

(2) (a) Stryer, L. *Biochemistry*, 4th ed.; W. H. Freeman and Co.: New York, 1995. (b) Datta, A.; Davis, D.; Sreekumar, K.; Pati, S. K. *J. Phys. Chem. A* **2005**, *109*, *4112*. (c) Asha, S. K.; Kavita, K.; Das, P. K.; Ramakrishnan, S. *Chem. Mater.* **1999**, *11*, 3352.

(3) March, J. *Advanced Organic Chemistry: Reactions, Mechanisms and Structure*, 4th ed.; John Wiley and Sons: New York, 1992.

(4) (a) Pophristic, V.; Goodman, L. *Nature* **2001**, *411*, 565−568. (b) Weinhold, F. *Nature* **2001**, *411*, 539−541.

(5) Weinhold, F. *Angew. Chem., Int. Ed.* **2003**, *42*, 4188−4194.

(6) Song, L.; Lin, Y.; Wu, W.; Zhang, Q.; Mo, Y. *J. Phys. Chem. A* **2005**, *109*, 2310−2316.

(7) Bickelhaupt, F. M.; Jan Baerends, E. *Angew. Chem., Int. Ed.* **2003**, *42*, 4183−4188.

(8) Mo, Y.; Wu, W.; Song, L.; Lin, M.; Zhang, Q.; Gao, J. *Angew. Chem., Int. Ed.* **2004**, *43*, 1986−1990.

(9) Tanwar, A.; Pal, S. *J. Phys. Chem. A* **2004**, *108*, 11838−11845.

(10) Marsh, C. M. B.; Hamilton, T. P.; Xie, Y.; Schaefer, H. F., III. *J. Chem. Phys.* **1992**, *96*, 5310−5317.

(11) Leboeuf, M.; Russo, N.; Salahub, D. R.; Toscano, M. *J. Chem. Phys.* **1995**, *103*, 7408−7413.

(12) Timoshkin, A. Y.; Suvorov, A. V.; Bettinger, H. F.; Schaefer, H. F., III. *J. Am. Chem. Soc.* **1999**, *121*, 5687−5699.

(13) Mo, Y.; Song, L.; Wu, W.; Zhang, Q. *J. Am. Chem. Soc.* **2004**, *126*, 3974−3982.

(14) Anane, H.; Boutalib, A.; Nebot-Gil, I.; Tomas, F. *J. Phys. Chem. A* **1998**, *102*, 7070−7073.

(15) Horvath, V.; Kovacs, A.; Hargittai, I. *J. Phys. Chem. A* **2003**, *107*, 1197−1202.

(16) Dillen, J.; Verhoeven, P. *J. Phys. Chem. A* **2003**, *107*, 2570−2577.

(17) Frisch, M. J.; Trucks, G. W.; Schlegel, H. B.; Scuseria, G. E.; Robb, M. A.; Cheeseman, J. R.; Montgomery, J. A., Jr.; Vreven, T.; Kudin, K. N.; Burant, J. C.; Millam, J. M.; Iyengar, S. S.; Tomasi, J.; Barone, V.; Mennucci, B.; Cossi, M.; Scalmani, G.; Rega, N.; Petersson, G. A.; Nakatsuji, H.; Hada, M.; Ehara, M.; Toyota, K.; Fukuda, R.; Hasegawa, J.; Ishida, M.; Nakajima, T.; Honda, Y.; Kitao, O.; Nakai, H.; Klene, M.; Li, X.; Knox, J. E.; Hratchian, H. P.; Cross, J. B.; Bakken, V.; Adamo, C.; Jaramillo, J.; Gomperts, R.; Stratmann, R. E.; Yazyev, O.; Austin, A. J.; Cammi, R.; Pomelli, C.; Ochterski, J. W.; Ayala, P. Y.; Morokuma, K.; Voth, G. A.; Salvador, P.; Dannenberg, J. J.; Zakrzewski, V. G.; Dapprich, S.; Daniels, A. D.; Strain, M. C.; Farkas, O.; Malick, D. K.; Rabuck, A. D.; Raghavachari, K.; Foresman, J. B.; Ortiz, J. V.; Cui, Q.; Baboul, A. G.; Clifford, S.; Cioslowski, J.; Stefanov, B. B.; Liu, G.; Liashenko, A.; Piskorz, P.; Komaromi, I.; Martin, R. L.; Fox, D. J.; Keith, T.; Al-Laham, M. A.; Peng, C. Y.; Nanayakkara, A.; Challacombe, M.; Gill, P. M. W.; Johnson, B.; Chen, W.; Wong, M. W.; Gonzalez, C.; Pople, J. A. *Gaussian 03*, revision B.05; Gaussian, Inc., Pittsburgh, PA, 2003.

(18) (a) Møller, C.; Plesset, M. S. *Phys. Rev.* **1934**, *46*, 618. (b) Becke, A. D. *J. Chem. Phys.* **1993**, *98*, 5648−5652. (c) Lee, C.; Yang, W.; Parr, R. G. *Phys. Rev. B* **1988**, *37*, 785−789.

(19) (a) Pearson, R. G. *J. Am. Chem. Soc.* **1963**, *85*, 3533−3539. (b) Pearson, R. G.; Songstad, J. *J. Am. Chem. Soc.* **1967**, *89*, 1827−1836.

(20) Pearson, R. G. *Inorg. Chem.* **1988**, *27*, 734−740.

(21) (a) Lowe, J. P. *J. Am. Chem. Soc.* **1970**, *92*, 3879−3800. (b) Lowe, J. P. *Science* **1973**, *179*, 527−532.

(22) (a) Fink, W. H.; Allen, L. C. *J. Chem. Phys.* **1967**, *46*, 2276−2284. (b) Fink, W. H.; Pan, D. C.; Allen, L. C. *J. Chem. Phys.* **1967**, *47*, 895−905. (c) Davidson, R. B.; Allen, L. C. *J. Chem. Phys.* **1971**, *54*, 2828−2830.

(23) Huheey, J. E.; Keiter, E. A.; Keiter, R. L. *Inorganic Chemistry: Principles of Structure and Reactivity*: Addison-Wesley: New York, 1993.

(24) Cotton, F. A.; Wilkinson, G.; Murillo, C. A.; Bochmann, M. *Advanced Inorganic Chemistry*, 6th ed.; John Wiley and Sons: New York, 2003.

(25) Vogler, A.; Kunkely, H. *Coord. Chem. Rev.* **2002**, *230*, 243−251.

(26) Pacchioni, G.; Bagus, P. S. *Inorg. Chem.* **1992**, *31*, 4391−4398.

(27) (a) *Charge and Energy Transfer Dynamics in Molecular System*; May, V., Kuhn, O., Eds.; Wiley-VCH: Berlin, 2000. (b) Aviram, A.; Ratner, M. A. *Chem. Phys. Lett.* **1974**, *29*, 277.